analytical chemistry

Article

pubs.acs.org/ac

Fully Automated Portable Comprehensive 2-Dimensional Gas Chromatography Device

Jiwon Lee,[†,‡] Menglian Zhou,[†,‡] Hongbo Zhu,[†,‡] Robert Nidetz,[‡,§] Katsuo Kurabayashi,[‡,§] and Xudong Fan*[,†,‡]

[†]Department of Biomedical Engineering, University of Michigan, 1101 Beal Avenue, Ann Arbor, Michigan 48109, United States

[‡]Center for Wireless Integrated MicroSensing and Systems (WIMS^2), University of Michigan, Ann Arbor, Michigan 48109, United States

[§]Department of Mechanical Engineering, University of Michigan, 2350 Hayward, Ann Arbor, Michigan 48109, United States

Supporting Information

ABSTRACT: We developed a fully automated portable 2-dimensional (2-D) gas chromatography (GC x GC) device, which had a dimension of 60 cm × 50 cm × 10 cm and weight less than 5 kg. The device incorporated a micropreconcentrator/injector, commercial columns, micro-Deans switches, microthermal injectors, microphotoionization detectors, data acquisition cards, and power supplies, as well as computer control and user interface. It employed multiple channels (4 channels) in the second dimension (^{2}D) to increase the ^{2}D separation time (up to 32 s) and hence ^{2}D peak capacity. In addition, a nondestructive flow-through vapor detector was installed at the end of the ^{1}D column to monitor the eluent from ^{1}D and assist in reconstructing ^{1}D elution peaks. With the information obtained jointly from the ^{1}D and ^{2}D detectors, ^{1}D elution peaks could be reconstructed with significantly improved ^{1}D resolution.

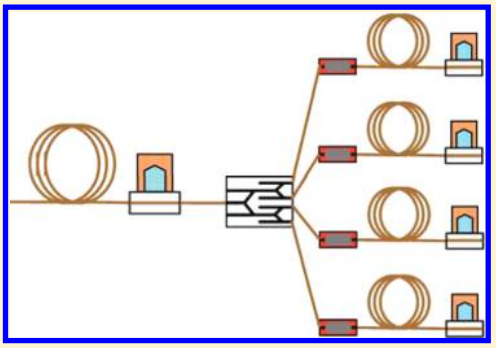

In this Article, we first discuss the details of the system operating principle and the algorithm to reconstruct ^{1}D elution peaks, followed by the description and characterization of each component. Finally, 2-D separation of 50 analytes, including alkane (C_6−C_{12}), alkene, alcohol, aldehyde, ketone, cycloalkane, and aromatic hydrocarbon, in 14 min is demonstrated, showing the peak capacity of 430−530 and the peak capacity production of 40−80/min.

Since the pioneering work by Terry et al.,[1] portable gas chromatography (GC) systems have been intensively investigated for a broad range of field applications such as environmental (air, water, and soil), chemical (explosive vapors, and chemical warfare agents), pharmaceutical or clinical (urine), and anthropogenic (indoor gas and operation) gas monitoring.[2−18] However, current portable GC systems, particularly those that have been commercialized such as Photovac Voyager GC (Photovac Inc.), Portable zNose (Electronic Sensor Technology), SeaPORT Mini-GC (Seacoast Science Inc.), 490 Micro GC (Agilent Technologies), FROG-4000 (Defiant Technologies), and 3000 Micro GC Gas Analyzer (Inficon) are simply miniaturized versions of the one-dimensional (1-D) benchtop GC. While field-deployable and rapid in vapor analysis, they suffer severely from deteriorated separation capability or peak capacity due primarily to the short column length, wide peak width resulting from miniaturization, and requirement for short analysis time. Therefore, they usually can separate only a small set or limited, well-defined class of vapors (such as chlorinated alkenes)[8] and often fail when complex sample matrixes or analyte mixtures are present.

Comprehensive two-dimensional (2-D) GC (i.e., GC × GC) is a technique that is developed to improve the peak capacity over 1-D GC. In GC × GC, a long first-dimensional (^{1}D) column, usually coated with a nonpolar stationary phase, is connected to a short second-dimensional (^{2}D) column that is usually coated with a polar stationary phase.[19−23] A modulator is placed between the two columns. It cuts the eluents from the ^{1}D column periodically (modulation period (P_M), ∼1−10 s[24,25]) and then reinjects each sliced segment into the ^{2}D column sequentially.[26] Consequently, each analyte is subject to two independent separation processes, first by its vapor pressure in the ^{1}D column and then by its polarity in the ^{2}D column. A 2-D chromatogram consisting of the ^{1}D and ^{2}D retention times can be reconstructed by analyzing the eluted peaks detected by a vapor detector installed at the end of the ^{2}D column. Ideally, the total peak capacity of GC × GC is $n_{GC\times GC} = n_1 \times n_2$, where n_1 and n_2 are the peak capacity for ^{1}D and ^{2}D separation, respectively.

To date, the predominant efforts in GC × GC have been dedicated to benchtop systems. The research work related to portable GC × GC has been focused mainly on developing miniaturized components, in particular miniaturized modulators. No actual portable or miniaturized GC × GC instrument

Received: August 3, 2016
Accepted: September 26, 2016
Published: October 6, 2016

DOI: 10.1021/acs.analchem.6b03000
Anal. Chem. 2016, 88, 10266−10274

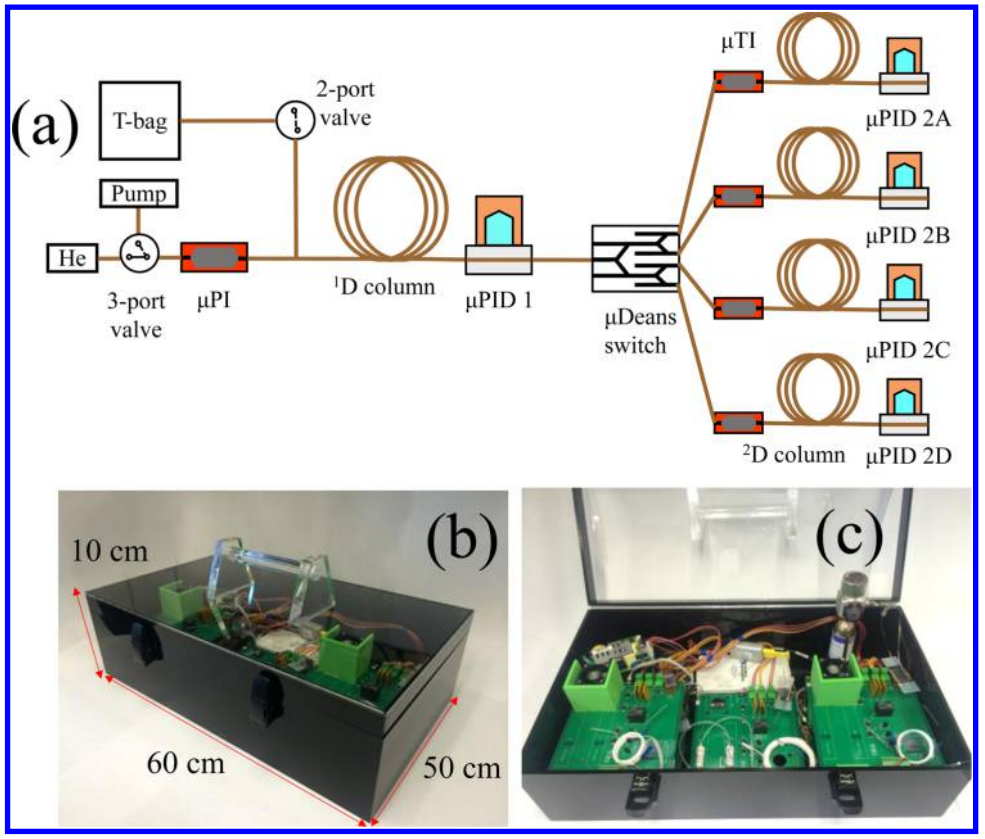

Figure 1. (a) Schematic of the portable 1 × 4−channel GC × GC device. (b and c) Photos of outside and inside of the device. The detailed device layout is shown in Figure S1.

has yet been reported. In 2009, Whiting et al. demonstrated the miniaturized pneumatic modulator based on microvalves.[27] While simple and responsive, the pneumatic modulator lacks the refocusing capability as seen in a thermal modulator, thus resulting in peak broadening in ^{2}D separation and decreased detection sensitivity. On the basis of the above modulator, a crude 2-D separation of 5 analytes was achieved using a conventional benchtop GC system. More recently, a microscale thermal modulator incorporating two series-coupled Pyrex-on-Si microchannels coated with a thin layer (0.3 μm) of polydimethylsiloxane (PDMS) was reported.[28−31] It employs a thermoelectric cooler (TEC) to cryogenically trap the analytes eluted from the ^{1}D column and refocuses and thermally injects them into the ^{2}D column.[28] The thermal modulator can be heated from −30 °C to ∼210 °C at a rate of 2400 °C/s, thus generating a peak as narrow as ∼100 ms (full-width-at-half-maximum, fwhm).[31] A hybrid GC × GC system was constructed using this microscale thermal modulator and the columns microfabricated on silicon wafers (6 and 0.5 m long for the ^{1}D and ^{2}D, respectively) as well as macroscopic injector, flame ionization detector, and GC oven on a conventional benchtop GC, showing 2-D separation of 36 analytes in 22 min. However, this type of thermal modulator faces several challenges, such as thermal crosstalk that may affect the trapping efficiency, bleeding of the coating materials (currently PDMS) at high temperature (currently the highest temperature is 210 °C), and breakthrough of highly volatile compounds (such as benzene).[31] Furthermore, constant cooling of the thermal modulator using a TEC requires a power of 20−40 W. Finally, its GC × GC architecture is still the same as that of the regular benchtop GC × GC, thus retaining the same limitations commonly seen in all existing GC × GC systems, i.e., degraded ^{1}D peak capacity due to peak broadening caused by modulation and insufficient ^{2}D separation capability arising from short maximally allowed ^{2}D separation time imposed by the modulation period (e.g., 6 s in ref 31).[32,33]

Here we demonstrated for the first time a fully automated portable comprehensive 2-D GC device. As illustrated in Figure 1a, our portable GC × GC device employed multiple channels in ^{2}D to increase the ^{2}D separation time (up to 32 s) and hence the ^{2}D peak capacity, and a nondestructive flow-through vapor detector was installed at the end of the ^{1}D column to monitor the ^{1}D separation and assist in reconstructing ^{1}D elution peaks. The entire device consisted of a microPreconcentrator/injector (μPI), commercial column (which can be replaced with microfabricated columns in the future), micro-Deans switch (μDS), microthermal injector (μTI), and microphotoionization detector (μPID), as well as miniaturized valve, pump, helium cartridge, and power supply. A Labview based user interface and operation control was also implemented for automation.

Operating Principle of Multichannel GC × GC. The general operating principle of the multichannel GC × GC is illustrated in Figure 1a. The analytes are first separated by the ^{1}D column and the elution is monitored by a nondestructive detector installed at the end of the ^{1}D column without interrupting the flow. A switching module is used to periodically send slices of eluents from the ^{1}D column to the multiple ^{2}D columns sequentially. The eluents from the ^{2}D columns are detected at the end of the columns. The ^{1}D elution peaks can be reconstructed from the information obtained jointly by the detectors in ^{1}D and ^{2}D (see details in Algorithm

DOI: 10.1021/acs.analchem.6b03000
Anal. Chem. 2016, 88, 10266−10274

for Reconstructing 1D Peaks). In this Article, we used a 1 × 4-channel GC × GC arrangement, as shown in Figure 1a. It had the following modules and operation processes.

(1) Sampling and injection module, which consisted of a Tedlar bag, a μPI, a pump, a 2-port valve, and a 3-port valve. The gas analytes from the Tedlar bag were first drawn by the pump through the 2-port valve into the μPI. Then, the μPI was heated to inject the analytes into the ^{1}D column.

(2) ^{1}D separation and detection module, which consisted of a home-built temperature programmable separation column and a vapor detector (PID 1).

(3) Modulation and switching module, which consisted of 3 μDSs to sequentially send the eluent from the ^{1}D column into one of the four ^{2}D columns, i.e., columns 2A, 2B, 2C, 2D, and then back to 2A.

(4) Four identical ^{2}D separation and detection modules, each of which consisted of a μTI, a temperature programmable column, and a vapor detector (PID 2A, 2B, 2C, and 2D). During operation, a slice of the ^{1}D eluent routed by the μDS was trapped by the μTI, which was then heated to inject the analyte into the ^{2}D column. Meanwhile, the slices from the ^{1}D eluent were routed to the remaining three ^{2}D columns. Therefore, the total separation time on each ^{2}D column could be as long as 4 times the modulation period.

Compared to the conventional GC × GC, our GC × GC design has several advantages. First, in the conventional GC × GC, the ^{2}D separation time is limited by the short modulation period (to avoid the wrap-around issue), thus resulting in the lower ^{2}D peak capacity. In contrast, the multiple channel design allows for much longer separation time to significantly increase the ^{2}D peak capacity. Furthermore, the increased ^{2}D separation time allows the μTIs to cool down slowly, thus avoiding the use of bulky and/or power intensive refrigeration mechanisms (such as TEC or liquid nitrogen). Second, in the conventional GC × GC, the ^{1}D elution peaks are not detected directly. Rather, they are reconstructed using the modulation period and the information obtained by the detector at the end of the ^{2}D column, which leads to deteriorated resolution (and hence lower ^{1}D peak capacity).[33] In contrast, in our GC × GC, PID 1 can monitor the ^{1}D elution so that the ^{1}D peaks can be reconstructed more accurately, thus increasing the ^{1}D peak capacity. Third, in comparison with the microscale thermal injector discussed previously, the modulation, focusing, and injection of analytes are accomplished by the μDS and the μTI, which are mechanically robust and can be operated at room temperature without the need for a TEC. Neither coating bleeding nor analyte breakthrough occurs. Fourth, our GC × GC system is highly scalable by adding more μDSs, μTIs, μPIDs, and ^{2}D columns. Finally, it exhibits high versatility to operate in a heart-cutting mode with minimal modifications (only in control software). Despite the aforementioned advantages, there are 2 major drawbacks to the multichannel GC × GC, i.e., the system complexity is higher and all the μPIDs must be calibrated against each other.[34]

Algorithm for Reconstructing ^{1}D Peaks. While in theory GC × GC enhances the peak capacity, in practice the enhancement is significantly impaired due to the lack of ^{1}D separation information.[33] The ^{1}D peaks are deduced from the information obtained from ^{2}D chromatograms. Several methods such as chemometrics have been explored,[35,36] but the ^{1}D reconstruction capability is still limited.

Here we demonstrate a reconstruction method of ^{1}D peaks using the exponentially modified Gaussian (EMG) model with the assist of the ^{1}D chromatogram obtained by PID 1. The EMG function, which begins with a Gaussian distribution and ends with an exponential decay, is widely used to analyze peaks in chromatography.[36−38] It can be defined as

$$f(t;\mu,\sigma,\lambda) = \frac{\lambda}{2}\exp\left[\frac{\lambda}{2}(2\mu+\lambda\sigma^2-2t)\right]\operatorname{erfc}\left(\frac{\mu+\lambda\sigma^2-t}{\sqrt{2}\sigma}\right) \quad (1)$$

where t is the time. λ is the rate of an exponential decay. μ and σ are the mean and the standard deviation of a normal Gaussian function, respectively. erfc is the complementary error function and defined as

$$\operatorname{erfc}(x) = \frac{2}{\sqrt{\pi}}\int_x^\infty e^{-q^2}\,dq \quad (2)$$

Note that the total area under the EMG function defined in eq 1 is normalized to unity. The retention time (t_m), i.e., the apex, of the EMG is defined as

$$t_m = \mu - \sqrt{2}\sigma\,\operatorname{erfcinv}\left(\frac{\sqrt{2}}{\sqrt{\pi}|\lambda|\sigma}\right) + \lambda\sigma^2 \quad (3)$$

where erfcinv is the inverse function of erfc.

Assuming that an analyte from ^{1}D is modulated to ^{2}D n times at t_1, t_2, t_3, ..., t_n and that the corresponding normalized peak area in ^{2}D is a_1, a_2, a_3, ..., a_n (i.e., $a_1 + a_2 + a_3 + ... + a_n = 1$). To find the best fit EMG curve for this analyte in ^{1}D, we establish an objective function, e, defined as follows

$$e = \sum_{i=1}^{n} e_i^2 \quad (4)$$

$$e_i = a_i - \int_{t_{i-1}}^{t_i} f(t;\mu,\sigma,\lambda)\,dt \quad (i = 1, 2, 3, ..., n) \quad (5)$$

Once the three parameters (μ, σ, and λ) are given, the normalized EMG function $f(t;\mu,\sigma,\lambda)$ is fully defined. To find μ, σ, and λ, we further assume that the retention time for the analyte is located between t_0 and t_n, i.e., $t_0 < t_m < t_n$, which allows us to scan t_m within the range of t_0 and t_n to find the optimal μ, σ, and λ. For a given t_m, there are only two independent parameters, σ and λ (μ can be determined by eq 3). Therefore, minimizing the objective function e in the σ−λ plane results in e_{min}, a set of (μ, σ, and λ), and hence the corresponding EMG function $f(t;\mu,\sigma,\lambda)$. Repeating the same procedures by scanning t_m (i.e., $t_m^{(1)}$, $t_m^{(2)}$, ..., $t_m^{(p)}$, where p is the number of t_m's used in the scanning), we can obtain a series of e_{min} (i.e., $e_{min}^{(1)}$, $e_{min}^{(2)}$, ..., $e_{min}^{(p)}$) and the associated EMG functions, $f(t;\mu^{(1)},\sigma^{(1)},\lambda^{(1)})$, $f(t;\mu^{(2)},\sigma^{(2)},\lambda^{(2)})$, ..., and $f(t;\mu^{(p)},\sigma^{(p)},\lambda^{(p)})$.

In the traditional method that lacks of the ^{1}D detector, the best fit EMG function $f(t;\mu,\sigma,\lambda)$ is the one that corresponds to the lowest e_{min}. In contrast, with the information provided by the ^{1}D detector, the EMG functions and hence the ^{1}D peaks can be obtained with much higher accuracy and resolution. Assuming the ^{1}D chromatogram obtained with the ^{1}D detector is $h(t)$, the difference (E) between $h(t)$ and $f(t;\mu,\sigma,\lambda)$ is given as

$$E = \int_{t_0}^{t_n} |h(t) - Af(t;\mu,\sigma,\lambda)|\,dt \quad (6)$$

DOI: 10.1021/acs.analchem.6b03000
Anal. Chem. 2016, 88, 10266−10274

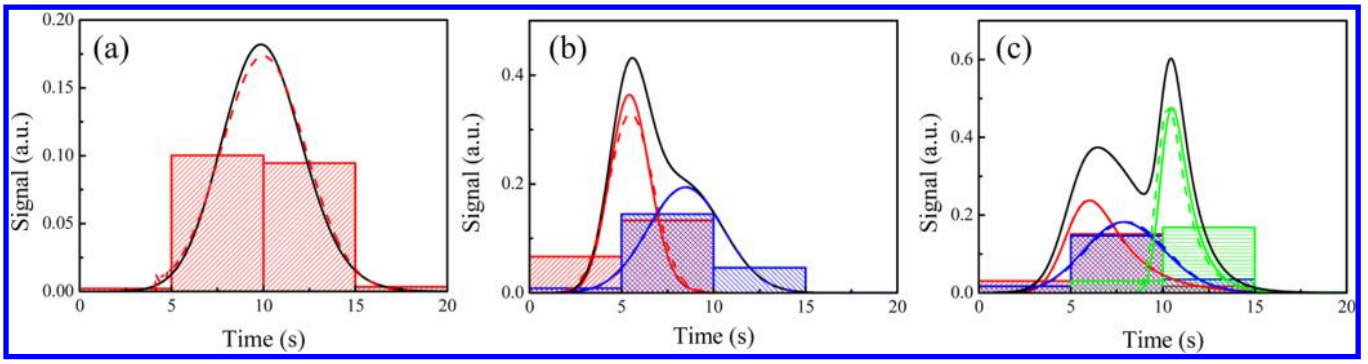

Figure 2. Computer simulation of ^{1}D reconstruction of (a) single peak, (b) coeluted two peaks, and (c) coeluted three peaks using the EMG model and the ^{1}D chromatogram detected by the ^{1}D detector. Black curves: ^{1}D chromatograms detected by the ^{1}D detector. Black curve in part a: μ = 9, σ = 2, and λ = 1 in eq 1. Red/blue solid curves in part b: 2 different analytes; μ = 5/7, σ = 1/2, and λ = 2/1 in eq 1. Red/blue/green solid curves in part c: 3 different analytes; μ = 5/7/10, σ = 1/2/0.5, and λ = 0.5/1/1 in eq 1. The combination of those curves results in the black curve in parts b and c. Red/blue/green dashed curves: reconstructed ^{1}D peaks using our algorithm. Red/blue/green bars: its width represents the modulation period (5 s in this case) and its area represents the analyte quantity of each modulation detected by the ^{2}D detector. For comparison, reconstruction of the same ^{1}D peaks without the ^{1}D chromatogram is shown in Figure S2.

where A represents the total area of the ^{2}D chromatograms. We test eq 6 with the p EMG functions obtained previously and the best fit EMG (and the associated area, A) is the one that minimizes E. Note that here we use the singlet case (there is only one analyte) in eq 6 to illustrate the algorithm for the sake of mathematical simplicity and completeness. In practice, if there is only one analyte, $h(t)$ itself can be used to reconstruct the ^{1}D peak. In the case of doublet (two coeluted analytes) and triplet (three coeluted analytes), eq 6 can be generalized as

$$E = \int_{t_0}^{t_n} |h(t) - A_j f(t; \mu_j, \sigma_j, \lambda_j) - A_k f(t; \mu_k, \sigma_k, \lambda_k)| \, dt \quad (7)$$

$$E = \int_{t_0}^{t_n} |h(t) - A_j f(t; \mu_j, \sigma_j, \lambda_j) - A_k f(t; \mu_k, \sigma_k, \lambda_k) - A_l f(t; \mu_l, \sigma_l, \lambda_l)| \, dt \quad (8)$$

where j, k, l = 1, 2, 3, ..., p for different coeluted analytes and $A_{j,k,l}$ are the corresponding total areas obtained from the ^{2}D chromatograms. By minimizing E, the best set of the EMG functions (along with the areas) for the coeluted analytes can be obtained.

In Figure 2, we simulated the reconstruction of one, two, and three coeluted peaks (singlet, doublet, and triplet) using the above algorithm. The corresponding ^{1}D reconstruction using the traditional method is shown in Figure S2. Note, as mentioned earlier, in practice singlet peaks can be reconstructed directly by the signal from the ^{1}D detector in our method. The singlet example presented in Figure 2a is simply to show the ability of our algorithm that contrasts the deficiencies in the traditional method. Below we use the doublet case to show in detail the reconstruction procedures. First, we arbitrarily generated the ^{1}D peaks with various combinations of μ, σ, and λ in eq 1. Red (μ = 5, σ = 1, and λ = 2) and blue (μ = 7, σ = 2, and λ = 1) solid curves in Figure 2b represent two analytes. The ^{1}D peaks were modulated every 5 s (P_M = 5 s) and the number of modulations was 4. Also, the scan step size was set to be 0.5 s and the t_m range was set from 0 to 20 s, so the number of possible retention time (t_m) was 40 (i.e., p = 40). Next, the ^{2}D peak areas were calculated (red and blue bars in Figure 2b). On the basis of eqs 1−5 and 7, the ^{1}D peaks were reconstructed and shown as red and blue dashed curves. Figure 2 shows that our algorithm is able to reconstruct the ^{1}D peaks with high accuracy. In contrast, as shown in Figure S2, the traditional method that uses the same EMG model but without the ^{1}D chromatogram (black curves) fails to accurately reconstruct the ^{1}D peaks (see red dashed curves in Figure S2a,b and the green dashed curve in Figure S2c).

EXPERIMENTAL SECTION

Materials. All the analytes used in the experiment were purchased from Sigma-Aldrich (St. Louis, MO) and Fisher Scientific (Pittsburgh, PA). They had purity greater than 97% and were used as received. Carbopack B (60−80 mesh) was purchased from Supelco (Bellefonte, PA). Disposable helium cartridge (95 mL, 2500 psig) was purchased from Leland (South Plainfield, NJ). GC guard columns (250 μm i.d. and 380 μm o.d.), Rtx-5MS (10 m × 250 μm i.d., 0.25 μm coating thickness), Rtx-200 (12 m × 250 μm i.d., 0.25 μm coating thickness), universal press-tight glass capillary column connectors, and angled Y-connectors were purchased from Restek (Belafonte, PA). The 2-port and 3-port solenoid valves were purchased from Lee Company (Westbrook, CT). A diaphragm pump was purchased from Gast Manufacturing (Benton Harbor, MI). Nickel wire (0.32 mm diameter, 1.24 Ω/m) was purchased from Lightning Vapes (Bradenton, FL). A type K thermocouple was purchased from Omega Engineering (Stamford, CT). A silicon wafer was purchased from University Wafer (Boston, MA). The UV lamps and amplifiers for PIDs were purchased from Baseline-Mocon (Lyons, CO). A 36 V ac/dc converter was purchased from TDK-Lambda Americas Inc. (National City, CA). A 24 V and a 12 V ac/dc converters and axial fans were purchased from Delta Electronics (Taipei, Taiwan). Data acquisition cards (DAQ cards), USB-6212 (16 bits) and USB-TC01 (for thermocouple measurement), were purchased from National Instruments (Austin, TX). Customized printed circuit board (PCB) was designed and manufactured by M.A.K.S., Inc. (Troy, MI). Duraseal silicone 1532 was purchased from Cotronics (Brooklyn, NY). Tubing (SFX.5-1.5) was purchased from Eldon James Corporation (Denver, CO).

Fabrication and Characterization of Components. *Fabrication/Characterization of μPI and μTI.* The μPI and μTI had a similar structure. Both consisted of a deep-reactive-ion-etched (DRIE) silicon cavity with tapered inlet/outlet

DOI: 10.1021/acs.analchem.6b03000
Anal. Chem. 2016, 88, 10266−10274

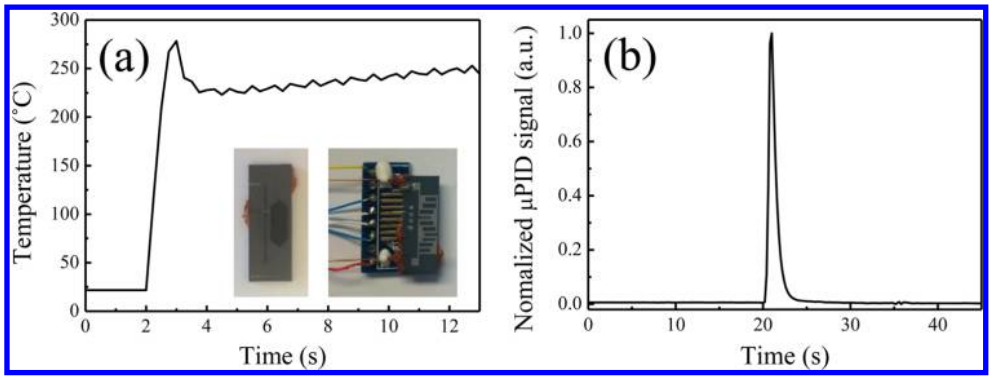

Figure 3. (a) Temperature response of the μPI. The μPI reached 270 °C in 0.6 s and then kept at 250 °C for 10 s. Inset shows the front and back side of the μPI packed with Carbopack B. At the back side, the heater and resistive temperature detector (RTD) were wire-bonded to a printed circuit board. (b) Normalized toluene peak obtained by PID 1 under the injection condition of part a. The helium flow rate was 2 mL/min, fwhm = 700 ms.

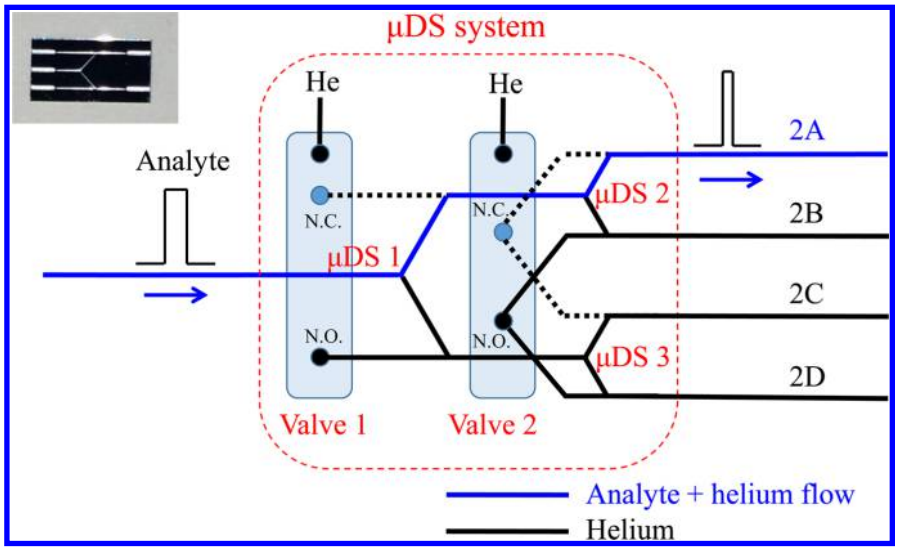

Figure 4. Schematic of the 1 × 4 flow switching module consisting of three μDSs (see the μDS picture in the inset) and two 3-port valves. The figure shows that the analyte is routed from the ^{1}D column to Column 2A in ^{2}D. The detailed μDS dimensions and the flow switching operation can be found in Figures S3 and S4.

ports, an integrated platinum heater, a temperature sensor, and microfluidic channels. The μPI had a cavity size of 8.15 mm × 2.9 mm × 0.25 mm, whereas μTI's cavity was slightly smaller (4.1 mm × 1.6 mm × 0.25 mm). Carbopack B granules were loaded into the cavity through a third port using a diaphragm pump, which was sealed with a silicon adhesive after loading. A small segment of guard column was inserted into the inlet and outlet fluidic ports and secured with an epoxy adhesive. For the electrical connections, the heater and resistive temperature detector (RTD) were wire-bonded to a printed circuit board (PCB). The RTD on the backside was precalibrated in a conventional GC oven at 50, 100, 150, and 200 °C to get the temperature calibration curve (i.e., temperature response versus the resistance). The μPI and μTI were preconditioned at 300 °C for 12 h under helium flow before use.

The insets of Figure 3a show the front and back side of the μPI. The front side photograph clearly shows the well-packed Carbopack B in the cavity. The volume of the cavity was 5.5 mm^3 and the mass of Carbopack B was 1.135 mg. During operation, the μPI was heated by applying 36 VDC for 0.6 s and subsequently12 VDC for 10 s for complete desorption. To maintain the constant temperature for 10 s by 12 VDC, a pulse-width-modulated (PWM) signal 4.0-Hz square wave was applied to the heater power relay via USB-6212. Figure 3a shows that the μPI reached 270 °C in 0.6 s at the heating rate of 314 °C/s and then kept at 250 °C for 10 s. The normalized toluene peak injected under this condition is given in Figure 3b, showing an fwhm of 700 ms.

Columns and Temperature Ramping and Reading. The 10 m long Rtx-5MS column for ^{1}D (or the 3 m long Rtx-200 column for ^{2}D) and the nickel wire were placed in parallel, wrapped by a Teflon tape, and then coiled into a helix of 10 cm (or 5 cm for the Rtx-200 column) in diameter and 1 cm in height. A type K thermocouple was inserted into the gap between the coiled column to monitor the column temperature in real time via USB-TC01. To achieve a programmed temperature ramping profile, a pulse-width-modulated signal (4.0-Hz square wave) was applied to the heater power relay via USB-6212. The duty cycle of the square wave was calculated by a proportional-integral-derivative controller in the LabView program and updated every 0.4 s based on the set and measured temperature.

Fabrication and Operation of the μDS System. A switching system was used to route eluents from an upstream column to

DOI: 10.1021/acs.analchem.6b03000
Anal. Chem. 2016, 88, 10266−10274

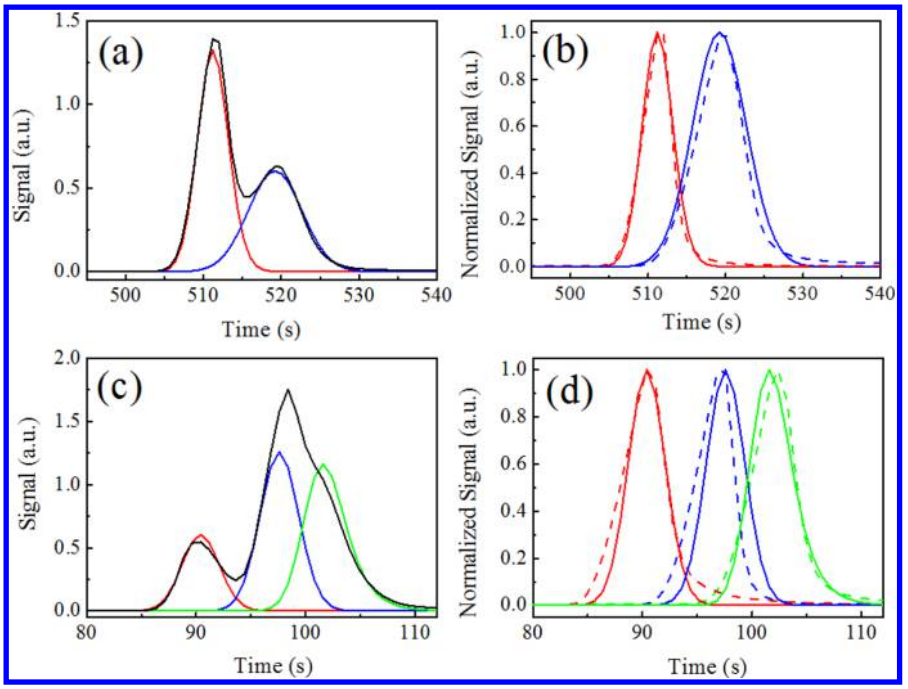

Figure 5. (a) ^{1}D chromatogram obtained with PID 1 for a mixture of 3-chlorotoluene and 1,3-dichlorobenzene (black curve). Reconstructed ^{1}D chromatogram for 3-chlorotoluene (red curve) and 1,3-dichlorobenzene (blue curve). (b) Comparison of the reconstructed ^{1}D chromatograms in (a) for 3-chlorotoluene and 1,3-dichlorobenzene (solid curves) and those obtained with PID 1 when 3-chlorotoluene and 1,3-dichlorobenzene were injected individually (dashed curves). All curves are normalized to their respective peaks for easy comparison. (c) ^{1}D chromatogram obtained with PID 1 for a mixture of heptane, 1,4-dioxane, and methylisobutylketone (black curve). Reconstructed ^{1}D chromatogram for heptane (red curve), 1,4-dioxane (blue curve), and methylisobutylketone (green curve). (d) Comparison of the reconstructed ^{1}D chromatograms in (a) for heptane, 1,4-dioxane, and methylisobutylketone (solid curves) and those obtained with μPID 1 when heptane, 1,4-dioxane, and methylisobutylketone were injected individually (dashed curves). All curves are normalized to their respective peaks for easy comparison.

one of the four downstream columns (1 × 4 switching). It consisted of three μDSs and two 3-port valves that were connected to a helium source as shown in Figure 4. The μDS, as shown in the inset of Figure 4, had a deep-reactive-ion-etched (DRIE) microfluidic channel (the dimension shown in Figure S3) with three inlets (on the left) and two outlets (on the right), an integrated platinum heater, and a temperature sensor. A small segment of guard column was inserted into the inlet and outlet fluidic ports, and secured with an epoxy adhesive. The middle inlet of the μDS was connected to the upstream column, whereas the other two inlets were connected to a 3-port valve (N.O. and N.C. port) for control helium gas to enter. The two outlets of μDS 1 were connected to the middle inlet of μDS 2 and μDS 3, respectively. As exemplified in Figure 4, in order to route a slice of an eluent from ^{1}D to Column 2A in ^{2}D, the two 3-port valves were operated in the "close" mode. The details of routing the analytes to other ^{2}D (2B and 2C) columns are given in Figure S4. During the operation, the flow rate was 2 mL/min for all ^{2}D channels.

Fabrication, Assembly, and Calibration of the μPID. The μPID module was assembled with the krypton UV lamp, the built-in lamp drive circuit, and the amplifier in a commercial PID from Baseline-Mocon (Lyons, CO, P/N 043-234), as well as a homemade flow-through ionization chamber. The μPID employed a 2 cm long straight microfluidic channel created by a 380 μm gap between two conductive silicon wafers with a thickness of 380 μm.[39] The bottom and top of the microfluidic channel was covered by a krypton UV lamp and a glass slide, respectively, which were then glued to the conductive silicon wafers with an optical epoxy. The effective UV illumination length in the channel was about 3.5 mm. Before use, the four μPIDs in ^{2}D were calibrated with toluene using PID 1 as the reference detector. The details of fabrication, characterization, calibration of the μPIDs were described in ref 34.

Device Assembly and Automation. Figure 1b,c shows the pictures of the portable GC × GC device. The system was housed in a customized plastic case and weighed less than 5 kg. All the modules were connected via tubings, universal connectors, and Y-connectors. The detailed layout of the device and a screen shot of the Labview user interface are shown in Figure S1a,b. Below we describe the operation procedures and parameters related to the experiments in this Article.

(1) The mixture of 50 analytes of 50 μg L^{-1} concentration placed in the Tedlar bag was drawn by the diaphragm pump through the 2-port valve and adsorbed by Carbopack B inside the μPI at a flow rate of 25 mL/min for 2 min. After sampling, the 2-port valve was closed, the helium gas was flowed through the 3-port valve for 60 s to stabilize the flow. Finally, the μPI was heated up to 270 °C in 0.6 s and then kept at 250 °C for 10 s for complete thermal desorption.

(2) The analyte underwent separation through the 10 m long Rtx-5MS column and then detected by PID 1. During the separation, the column was heated and kept at 50 °C for 1 min, then ramped at a rate of 5 °C min^{-1} to 120 °C, and kept at 120 °C for 4 min. PID 1 was kept at room temperature (25 °C). The flow rate was 2 mL/min.

(3) We used a modulation period of 8 s. The first 8 s long slice of the eluent from the ^{1}D column was routed to and trapped by μTI 2A, which were kept at room temperature (25 °C). Then the μTI was heated to 270 °C in 0.6 s and then kept at 250 °C for 5 s to inject the trapped analytes to Column 2A.

DOI: 10.1021/acs.analchem.6b03000
Anal. Chem. 2016, 88, 10266−10274

Immediately after the injection, the fan on the μTI 2A was turned on to rapidly lower the μTI back to room temperature in 16 s (see Figure S5). In the meantime, the second 8 s long slice of the eluent from the ^{1}D column was routed to and trapped by μTI 2B, which was subsequently injected into Column 2B. The same operation repeated for μTI 2C and μTI 2D, until the fifth 8 s long slice, which was routed to μTI 2A again. During the entire operation, the helium flow was 2 mL/min for all ^{2}D columns.

(4) The analyte underwent ^{2}D separation through one of the 3 m long Rtx-200 columns (kept at 60 °C during entire operation) and then detected by μPID 2 (kept at room temperature, 25 °C). During the separation, the helium flow rate was 2 mL/min. The maximal separation time for each ^{2}D column was 32 s (4 times the modulation period).

RESULTS

Reconstruction of ^{1}D Peaks. We validated the reconstruction method of ^{1}D peaks by injecting the sample into our device and comparing the experimental peaks with the reconstructed ones. Figure S6 shows the ^{2}D separation for singlet, doublet, and triplet. Note that the standard deviation of the retention times of each peak is shown in Figure S7. Here we use the doublet to illustrate the reconstruction of the ^{1}D peaks. In this case, 3-chlorotoluene and 1,3-dichlorobenzene were selected due to their similar ^{1}D retention time. The black curve in Figure 5a was detected by PID 1, showing that the two analytes were not fully separated. This ^{1}D peak was then modulated at 512, 520, 528, and 536 s and further separated in ^{2}D (see Figure S6b). The ^{1}D peaks were reconstructed according to the procedures described in Algorithm for Reconstructing 1D Peaks and shown as the red and blue curves in Figure 5a. To further verify the ^{1}D peak reconstruction, each of the two analytes was injected individually into our system. The corresponding comparison between the original peaks detected by PID 1 and those reconstructed is presented in Figure 5b. Similarly, the singlet and triplet in ^{1}D can be reconstructed and the corresponding results are shown in Figure S8 and Figure 5c,d, respectively. The above examples suggest that our device and the corresponding algorithm are able to accurately reconstruct ^{1}D peaks. Note that we present the singlet result to show the capability of our algorithm. In practice, we use the ^{1}D peak obtained directly from PID 1.

Contour Plot. Traditionally, the output of GC × GC is simply a long series of the ^{2}D chromatograms,[19,40] since there is no detector in ^{1}D. Thus, the resolution of the traditional 2-D contour plot is degraded due to the modulation and the lack of information on the ^{1}D chromatogram. In contrast, in our GC × GC, with the information obtained from the reconstructed ^{1}D peaks, the 2-D contour plot can be created with significantly increased resolution. To make such a 2-D contour plot, the ^{2}D chromatograms were first deconvoluted for each analyte. For analyte s, we can define its ^{1}D chromatogram as the area-normalized EMG function, $f_s(^1t_R)$, and the ^{2}D chromatogram as $g_s^{(v)}(^2t_R)$. $v = \left\lfloor \frac{^1t_R}{P_M} \right\rfloor + 1$ (= 1, 2, ..., n) represents the vth modulation from ^{1}D to ^{2}D, where $\lfloor\cdot\rfloor$ is the floor function. Then, we can get the 2-D contour plot of $C_s(^1t_R, ^2t_R)$ as

$$C_s(^1t_R, ^2t_R) = f_s(^1t_R) g_s^{(v)}(^2t_R) \quad (9)$$

Correspondingly, the 2-D contour plot, $C(^1t_R, ^2t_R)$, of entire N analytes can be written as

$$C(^1t_R, ^2t_R) = \sum_{s=1}^{N} C_s(^1t_R, ^2t_R) \quad (10)$$

Figure S9 shows the 2-D and the 3-D contour plots for singlet, doublet, and triplet analytes in Figure S7 and Figure 5 using the method described in eqs 9 and 10, showing well resolved peaks. For comparison, corresponding the 2-D and 3-D contour plots using the traditional method are given in Figure S10.

Demonstration of 2-D Separation of 50 VOCs. We employed the portable 1 × 4-channel GC × GC device to analyze a mixture of 50 VOCs (see Table S1). First, the mixture of 50 VOCs, prepared in a Tedlar bag, was separated in ^{1}D and the corresponding ^{1}D chromatogram were recorded by PID 1 (see Figure S11). With the modulation period of 8 s, the analytes were routed to the ^{2}D separation modules and separated in ^{2}D. Figure 6 presents the 2-D contour plot of the

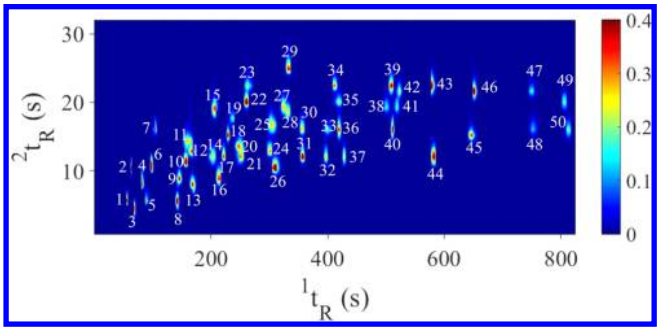

Figure 6. 2-D contour plot of the 50 VOCs generated with the portable 1 × 4-channel GC × GC device. The list of those VOCs is given in Table S1.

50 VOCs using the ^{1}D reconstruction and contour plot methods discussed in this Article. It can be seen that the 50 VOCs were completely separated in only 850 s (or 14.2 min). The corresponding reconstructed retention time and peak width in ^{1}D, and retention time and peak width in ^{2}D are listed in Table S1.

DISCUSSION AND CONCLUSION

For GC × GC, the peak capacity is defined as

$$n_{GC\times GC} = n_1 \times n_2 \quad (11)$$

where n_1 and n_2 are the peak capacity for ^{1}D and ^{2}D, respectively. With the chromatographic resolution Rs of 1, eq 11 can be written as[41]

$$n_{GC\times GC} = 0.35(^1t_R/^1\text{fwhm}) \times (CP_M/^2\text{fwhm}) \quad (12)$$

where ^1t_R is the analyte retention time in ^{1}D. ^{1}fwhm and ^{2}fwhm are the fwhm in ^{1}D and ^{2}D, respectively. P_M is the modulation period and C are the number of the ^{2}D channels. Correspondingly, the peak capacity production can be written as follows:[41]

$$n_{GC\times GC}/^1t_R = 0.35/^1\text{fwhm} \times (CP_M/^2\text{fwhm}) \quad (13)$$

Here, we evaluate the 1 × 4-channel GC × GC performance using three exemplary analytes, 2-ethoxyethyl acetate, benzaldehyde, and dodecane. Table S2 presents the peak capacity and

DOI: 10.1021/acs.analchem.6b03000
Anal. Chem. 2016, 88, 10266−10274

peak capacity production of 2-ethoxyethyl acetate, benzaldehyde, and dodecane. The peak capacity production ranges from 40/min to 80/min, similar to that in a conventional GC × GC.[33,41−44]

In summary, we have developed the first of its kind, fully automated, portable 1 × 4-channel GC × GC device. The device is compact and robust and provides excellent peak capacity and peak capacity production. In the future, the device can be improved by increasing the ^{2}D flow rate, reducing ^{2}D column inner diameter and increasing the heating rate for μPI and μTI. More channels can also be added to increase ^{2}D separation time. The device size and weight can be further reduced by using microfabricated columns and by integrating different components (such as data acquisition cards, power supplies, valves, cables, tubings, and connectors) on the same chip or printed circuit board. We envision that the portable GC × GC will lead to a plethora of field applications in environmental monitoring and protection, workplace safety monitoring, winery, food industry, and biomedicine.[45−50]

■ ASSOCIATED CONTENT

Supporting Information

The Supporting Information is available free of charge on the ACS Publications website at DOI: 10.1021/acs.analchem.6b03000.

Experimental details and additional data (PDF)

■ AUTHOR INFORMATION

Corresponding Author

*E-mail: xsfan@umich.edu.

Notes

The authors declare no competing financial interest.

■ ACKNOWLEDGMENTS

We would like to thank Environmental Protection Agency (Grant 83564401) for financial support and the Lurie Nanofabrication Facility for fabrication assistance.

■ REFERENCES

(1) Jerman, J. H.; Terry, S. C. *Environ. Int.* **1981**, *5*, 77−83.
(2) Bond, E. J.; Dumas, T. *J. Agric. Food Chem.* **1982**, *30*, 986−988.
(3) Lorenzelli, L.; Benvenuto, A.; Adami, A.; Guarnieri, V.; Margesin, B.; Mulloni, V.; Vincenzi, D. *Biosens. Bioelectron.* **2005**, *20*, 1968−1976.
(4) Thompson, C. V.; Goedert, M. G. In *Encyclopedia of Analytical Chemistry*; John Wiley & Sons, Ltd.: Chichester, U.K., 2006.
(5) Ohira, S.-I.; Toda, K. *Anal. Chim. Acta* **2008**, *619*, 143−156.
(6) Liu, X.; Pawliszyn, J. *Int. J. Environ. Anal. Chem.* **2005**, *85*, 1189−1200.
(7) Mohsen, Y.; Lahlou, H.; Sanchez, J.-B.; Berger, F.; Bezverkhyy, I.; Weber, G.; Bellat, J.-P. *Microchem. J.* **2014**, *114*, 48−52.
(8) Jian, R.-S.; Wang, T.-Y.; Song, L.-Y.; Kuo, C.-Y.; Tian, W.-C.; Lo, E.-W.; Lu, C.-J. *Build. Environ.* **2015**, *94* (Part 1), 287−295.
(9) Akbar, M.; Shakeel, H.; Agah, M. *Lab Chip* **2015**, *15*, 1748−1758.
(10) Akbar, M.; Restaino, M.; Agah, M. *Microsyst. Nanoeng.* **2015**, *1*, 15039.
(11) Qin, Y.; Gianchandani, Y. B. *J. Microelectromech. Syst.* **2014**, *23*, 980−990.
(12) Qin, Y.; Gianchandani, Y. B. *J. Micromech. Microeng.* **2014**, *24*, 065011.
(13) Qin, Y.; Gianchandani, Y. B. *Microsys. Nanoeng.* **2016**, *2*, 15049.
(14) Bulbul, A.; Kim, H. *Lab Chip* **2015**, *15*, 94−104.
(15) Hsieh, H.-C.; Kim, H. *Lab Chip* **2016**, *16*, 1002−1012.
(16) Shopova, S. I.; White, I. M.; Sun, Y.; Zhu, H.; Fan, X.; Frye-Mason, G.; Thompson, A.; Ja, S.-j. *Anal. Chem.* **2008**, *80*, 2232−2238.
(17) Liu, J.; Sun, Y.; Howard, D. J.; Frye-Mason, G.; Thompson, A. K.; Ja, S.-j.; Wang, S.-K.; Bai, M.; Taub, H.; Almasri, M.; Fan, X. *Anal. Chem.* **2010**, *82*, 4370−4375.
(18) Jian, R.-S.; Huang, Y.-S.; Lai, S.-L.; Sung, L.-Y.; Lu, C.-J. *Microchem. J.* **2013**, *108*, 161−167.
(19) Dallüge, J.; Beens, J.; Brinkman, U. A. T. *J. Chromatogr. A* **2003**, *1000*, 69−108.
(20) Marriott, P. J.; Chin, S.-T.; Maikhunthod, B.; Schmarr, H.-G.; Bieri, S. *TrAC, Trends Anal. Chem.* **2012**, *34*, 1−21.
(21) Seeley, J. V.; Seeley, S. K. *Anal. Chem.* **2012**, *85*, 557−578.
(22) Seeley, J. V.; Seeley, S. K. *Anal. Chem.* **2013**, *85*, 557−578.
(23) Chin, S.-T.; Marriott, P. J. *Chem. Commun.* **2014**, *50*, 8819−8833.
(24) Edwards, M.; Mostafa, A.; Górecki, T. *Anal. Bioanal. Chem.* **2011**, *401*, 2335−2349.
(25) Pursch, M.; Sun, K.; Winniford, B.; Cortes, H.; Weber, A.; McCabe, T.; Luong, J. *Anal. Bioanal. Chem.* **2002**, *373*, 356−367.
(26) Dallüge, J.; Beens, J.; Brinkman, U. A. T. *J. Chromatogr. A* **2003**, *1000*, 69−108.
(27) Whiting, J. J.; Fix, C. S.; Anderson, J. M.; Staton, A. W.; Manginell, R. P.; Wheeler, D. R.; Myers, E. B.; Roukes, M. L.; Simonson, R. J. In *TRANSDUCERS 2009 - 2009 International Solid-State Sensors, Actuators and Microsystems Conference*, Denver, CO, June 21−25, 2009; pp 1666−1669.
(28) Kim, S. J.; Reidy, S. M.; Block, B. P.; Wise, K. D.; Zellers, E. T.; Kurabayashi, K. *Lab Chip* **2010**, *10*, 1647−1654.
(29) Serrano, G.; Paul, D.; Kim, S.-J.; Kurabayashi, K.; Zellers, E. T. *Anal. Chem.* **2012**, *84*, 6973−6980.
(30) Kim, S.-J.; Serrano, G.; Wise, K. D.; Kurabayashi, K.; Zellers, E. T. *Anal. Chem.* **2011**, *83*, 5556−5562.
(31) Collin, W. R.; Bondy, A.; Paul, D.; Kurabayashi, K.; Zellers, E. T. *Anal. Chem.* **2015**, *87*, 1630−1637.
(32) Blumberg, L. M. *Anal. Chem.* **2002**, *74*, 503A.
(33) Blumberg, L. M.; David, F.; Klee, M. S.; Sandra, P. *J. Chromatogr. A* **2008**, *1188*, 2−16.
(34) Lee, J.; Zhou, M.; Zhu, H.; Nidetz, R.; Kurabayashi, K.; Fan, X. *Analyst* **2016**, *141*, 4100−4107.
(35) Zeng, Z.-D.; Hugel, H. M.; Marriott, P. J. *J. Sep. Sci.* **2013**, *36*, 2728−2737.
(36) Kong, H.; Ye, F.; Lu, X.; Guo, L.; Tian, J.; Xu, G. *J. Chromatogr. A* **2005**, *1086*, 160−164.
(37) Jeansonne, M. S.; Foley, J. P. *J. Chromatogr. Sci.* **1991**, *29*, 258−266.
(38) Jung, K. H.; Yun, S. J.; Kang, S. H. *Anal. Chem.* **1984**, *56*, 457−462.
(39) Zhu, H.; Nidetz, R.; Zhou, M.; Lee, J.; Buggaveeti, S.; Kurabayashi, K.; Fan, X. *Lab Chip* **2015**, *15*, 3021−3029.
(40) Kallio, M.; Hyötyläinen, T. *J. Chromatogr. A* **2007**, *1148*, 228−235.
(41) Siegler, W. C.; Crank, J. A.; Armstrong, D. W.; Synovec, R. E. *J. Chromatogr. A* **2010**, *1217*, 3144−3149.
(42) Sinha, A. E.; Prazen, B. J.; Fraga, C. G.; Synovec, R. E. *J. Chromatogr. A* **2003**, *1019*, 79−87.
(43) Fitz, B. D.; Wilson, R. B.; Parsons, B. A.; Hoggard, J. C.; Synovec, R. E. *J. Chromatogr. A* **2012**, *1266*, 116−123.
(44) Klee, M. S.; Cochran, J.; Merrick, M.; Blumberg, L. M. *J. Chromatogr. A* **2015**, *1383*, 151−159.
(45) Pani, O.; Górecki, T. *Anal. Bioanal. Chem.* **2006**, *386*, 1013−1023.
(46) Beens, J.; Dallüge, J.; Adahchour, M.; Vreuls, R. J. J.; Brinkman, U. A. T. *J. Microcolumn Sep.* **2001**, *13*, 134−140.
(47) Lewis, A. C.; Carslaw, N.; Marriott, P. J.; Kinghorn, R. M.; Morrison, P.; Lee, A. L.; Bartle, K. D.; Pilling, M. J. *Nature* **2000**, *405*, 778−781.
(48) Weldegergis, B. T.; Villiers, A. d.; McNeish, C.; Seethapathy, S.; Mostafa, A.; Górecki, T.; Crouch, A. M. *Food Chem.* **2011**, *129*, 188−199.
(49) Tranchida, P. Q.; Dugo, P.; Dugo, G.; Mondello, L. *J. Chromatogr. A* **2004**, *1054*, 3−16.

DOI: 10.1021/acs.analchem.6b03000
Anal. Chem. 2016, 88, 10266−10274

(50) Phillips, M.; Cataneo, R. N.; Chaturved, A.; Kaplan, P. D.; Libardoni, M.; Mundada, M.; Patel, U.; Zhang, X. *PLoS One* **2013**, *8*, e75274.

DOI: 10.1021/acs.analchem.6b03000
Anal. Chem. 2016, 88, 10266−10274